ENVIRONMENTAL RESEARCH
LETTERS

PURPOSE-LED PUBLISHING™

LETTER • **OPEN ACCESS**

Thermal changes along the urban-rural continuums in Southeast Asia

To cite this article: Yuanhui Zhu *et al* 2025 *Environ. Res. Lett.* **20** 054051

View the article online for updates and enhancements.

You may also like

- Satellite-detected gain in built-up area as a leading economic indicator
Qing Ying, Matthew C Hansen, Laixiang Sun et al.
- Chemical Reaction Mechanism between A-Site Deficient La Substituted $SrTiO_3$ and PH_3 in Coal Syngas
Gang Chen, Haruo Kishimoto, Katsuhiko Yamaji et al.
- Multi-city analysis of satellite surface temperature compared to crowdsourced air temperature
Marzie Naserikia, Negin Nazarian, Melissa A Hart et al.



This content was downloaded from IP address 147.26.185.226 on 24/04/2025 at 13:55

IOP Publishing Environ. Res. Lett. 20 (2025) 054051 https://doi.org/10.1088/1748-9326/adcad2

ENVIRONMENTAL RESEARCH
LETTERS

CrossMark

OPEN ACCESS

RECEIVED
17 December 2024

REVISED
29 March 2025

ACCEPTED FOR PUBLICATION
9 April 2025

PUBLISHED
23 April 2025

Original content from this work may be used under the terms of the Creative Commons Attribution 4.0 licence.

Any further distribution of this work must maintain attribution to the author(s) and the title of the work, journal citation and DOI.



LETTER

Thermal changes along the urban-rural continuums in Southeast Asia

Yuanhui Zhu[1,*], Soe W Myint[1,2], Jiquan Chen[3,4], Peilei Fan[5], Karen C Seto[6], Atul Jain[7], Jiaguo Qi[4] and Jin Wang[3]

[1] Department of Geography and Environmental Studies, Texas State University, San Marcos, TX, United States of America
[2] The Meadows Center for Water and the Environment, San Marcos, TX, United States of America
[3] Department of Geography, Environment, and Spatial Sciences, Michigan State University, East Lansing, MI, United States of America
[4] Center for Global Change and Earth Observations, Michigan State University, East Lansing, MI, United States of America
[5] Department of Urban and Environmental Policy and Planning, Tufts University, Medford, MA, United States of America
[6] Yale School of the Environment, Yale University, New Haven, CT, United States of America
[7] Department of Climate, Meteorology, and Atmospheric Sciences, University of Illinois, Urbana, IL, United States of America
[*] Author to whom any correspondence should be addressed.

E-mail: jta90@txstate.edu

Keywords: urban thermal variations, urban-rural continuums, Southeast Asia, urbanization, land use and land cover changes

Supplementary material for this article is available online

Abstract

Southeast Asia's (SEA) rapid urbanization has intensified urban heat effects. While previous studies address urban warming at specific time points, the dynamic relationship between land cover and land use (LCLU) changes and land surface temperature (LST) along urban-rural continuums remains understudied. This study examines LST, LCLU, and NDVI changes across 19 SEA cities of varying urbanization levels from 2000 to 2022 using Landsat images. Results show that LST change rates differ by urbanization levels, with built-up lands driving urban warming. Larger cities exhibited more intense and widespread LST increases extending into rural areas. The megacities experienced significant LST growth within 5 km of city centers despite limited built-up expansion. However, some areas in many cities experience decreasing trends of heat. NDVI significantly influenced LST changes through its cooling effect and the warming impact due to vegetation loss caused by urban expansion. Findings support urban planning strategies that balance growth with enhancing green spaces, redirecting growth to smaller cities, and shifting development from city centers to urban outskirts.

1. Introduction

Southeast Asia (SEA), home to 675 million people in 2021, represents 8.56% of the global population yet occupies only 3% of Earth's land [1]. Nearly half (49.63%) of SEA's population resides in urban areas, highlighting stark disproportion in densely populated urban environments. Between 1950 and 2014, the urban population surged 11-fold, from 26 million to 294 million [2]. This rapid growth, dense populations, and unique geographies make SEA cities highly vulnerable to global climate warming impacts [2]. Rising temperatures have intensified extreme weather events like heatwaves, floods, and cyclones, disrupting environmental, social, and economic systems [3, 4] and increasing heat-related mortality to projected rates of 200–300 deaths per 100 000 annually by 2030–2079 [5]. Therefore, understanding how rapid urbanization impacts thermal conditions and their spatiotemporal variations is crucial for effective planning and urban management.

Urbanization has been demonstrated to exacerbate urban warming significantly [6–9]. This effect in SEA manifests across the urban-rural continuums (URCs) [10, 11]. Although research has demonstrated the impact of land cover and land use (LCLU) changes on urban warming, many studies focus only on single time points (e.g. one specific year) [9, 12–17]. With the rapid pace of urbanization in SEA, the interactions between LCLU changes and urban thermal are increasingly dynamic and complex [18]. Understanding urban warming changes is crucial for

© 2025 The Author(s). Published by IOP Publishing Ltd

assessing the impacts of urbanization along the URCs [18]. However, little research has addressed how these urban warming patterns shift over time across the URCs.

City size, closely linked to urbanization level, strongly influences urban heat intensity, development patterns, and population density [11, 18–20]. While past studies have broadly linked city size to urban heat intensity, given that SEA cities vary widely in urbanization intensity and population density, there remains a gap in understanding distinct urban thermal variations across different levels of urbanization and how specific LCLU changes affect land surface temperature (LST) over time along URCs in SEA cities.

SEA cities are an emerging research hotspot due to the combined effects of climate warming, unplanned urbanization, and rapid LCLU changes [21]. Our study focuses on the URCs in SEA cities, where urban and rural elements blend, creating dynamic zones [11, 22]. This study aims to analyze the annual summer changes in LST using Landsat data and investigate how urbanization-driven LCLU changes have influenced LST dynamics across URCs from 2000 to 2022. Specifically, we address two key questions: (1) How have LST variations differed across cities with different urbanization levels? (2) What roles have LCLU changes played in driving LST shifts along the URCs over the past two decades? By answering these questions, this study aims to provide evidence-based insights for policymakers to integrate social and environmental considerations into more sustainable, locally adapted urban development strategies.

2. Materials and methods

2.1. Data description and processing

Our study focused on 19 cities across eight countries: Cambodia, Indonesia, Lao PDR, Malaysia, Myanmar, Philippines, Thailand, and Vietnam (table 1 and figure 1). These cities were selected to capture diverse urbanization levels, geographical diversity, and climatic conditions, enabling a robust analysis of urban thermal dynamics across varying city sizes and urban expansion rates [11, 18].). Based on UN DESA (2019) categories, the cities were grouped by population: Mega (>10 M), Large (1–10 M), Medium (250k–1 M), and Small (20–250 K) [23].

We utilized all available Landsat data (2000–2022) to retrieve 30 m resolution LST using the Statistical Mono-Window (SMW) algorithm [24–26] and calculated NDVI via Google Earth Engine for the summer months (June, July, and August) (table 2). 5,265 Landsat 5/7/8/9 scenes were collected to ensure complete coverage of all 19 cities. These images span from 2000 to 2022, apart from 2012, for which no single Landsat image was available. The number of Landsat images corresponding to each city is provided in table S1 of the Supplemental Materials. Contaminated pixels (e.g. clouds and cloud shadows) were removed via quality assessment bands, and Landsat-7 SLC-off stripes were eliminated.

LST is estimated from Landsat images using SMW algorithm, developed by the Climate Monitoring Satellite Application Facility [24]. This approach integrates atmospheric parameters and surface emissivity data. The SMW algorithm establishes an empirical linear relationship between LST and the top-of-atmosphere brightness temperature within a single thermal infrared window [25–27]. This model is derived by linearizing the radiative transfer equation, incorporating surface emissivity as a critical variable [28, 29].

LCLU data (table 2) with 30 m resolution for 2000, 2005, 2010, 2015, and 2020 were sourced from the University of Maryland [30]. These datasets include built-up lands, croplands, wetlands, vegetation, and water features such as rivers, lakes, and seas. Data were available for 2000, 2005, 2010, 2015, and 2020, with user and producer accuracies exceeding 85% for most categories except built-up lands (63.7% and 39.1% for stable built-up; 74.1% and 59.6% for built-up gains). We compared these global LCLU datasets with the European Space Agency Land Cover Climate Change Initiative at a 300 m resolution [31]. Our analysis revealed that former datasets proved more detailed and accurate, especially with regard to urban areas (figure S1 of the Supplemental Materials). Other datasets providing annual data were either incomplete, geographically limited, or posed risks of bias and uncertainty due to varying accuracy and classification methods.

2.2. Data analysis

To assess the impact of urbanization over the past two decades, we analyzed the patterns of LST changes with LCLU changes across 19 SEA cities along URCs. These cities range from major hubs like Jakarta and Bangkok to smaller cities like Vientiane and Chiang Rai, offering a diverse sample of SEA's urban environments and thermal impacts. URCs were defined as areas within a 30 km radius of each city center. City center points were identified as the central business district or geometric center of administrative limits [11]. We created 30 ring buffer zones at 1 km intervals to examine LCLU and LST gradients.

After establishing these buffer zones, we excluded (1) large water bodies or oceans; (2) continuous urban areas beyond the city boundaries—for neighboring cities like Kuala Lumpur and Putrajaya, and Quezon City and Taytay, we adjusted the URCs to exclude overlapping administrative boundaries. This ensured that the analysis focused on each city's designated URC, minimizing cross-boundary influences. For example, Quezon City's URC aligns with Taytay's urban extent, and excluding these overlapping urban areas improved the reliability of our results; (3)

Table 1. Selected urban centers across urban-rural continuums (URCs).

Country	Mega (>10 M)	Large (1–10 M)	Medium (250k–1 M)	Small (20–250 K)
Cambodia		Phnom Penh (2.3 M)		Siem Reap (249 K)
Indonesia	Jakarta (10.5 M)	Surabaya (2.8 M)	Denpasar (725 K)	
Lao PDR			Vientiane (969 K)	Pakse (88 K)
Malaysia		KL (1.8 M)		Putrajaya (109 K)
Myanmar		Yangon (5.1 M)	NPT (375 K)	
Philippines		Quezon City (2.7 M)	Iloilo (387 K)	Taytay (231 K)
Thailand		Bangkok (5.1 M)		Chiang Rai (79k)
Vietnam		HCMC (9.0 M), Hanoi (8 M)	Cantho (812 K)	

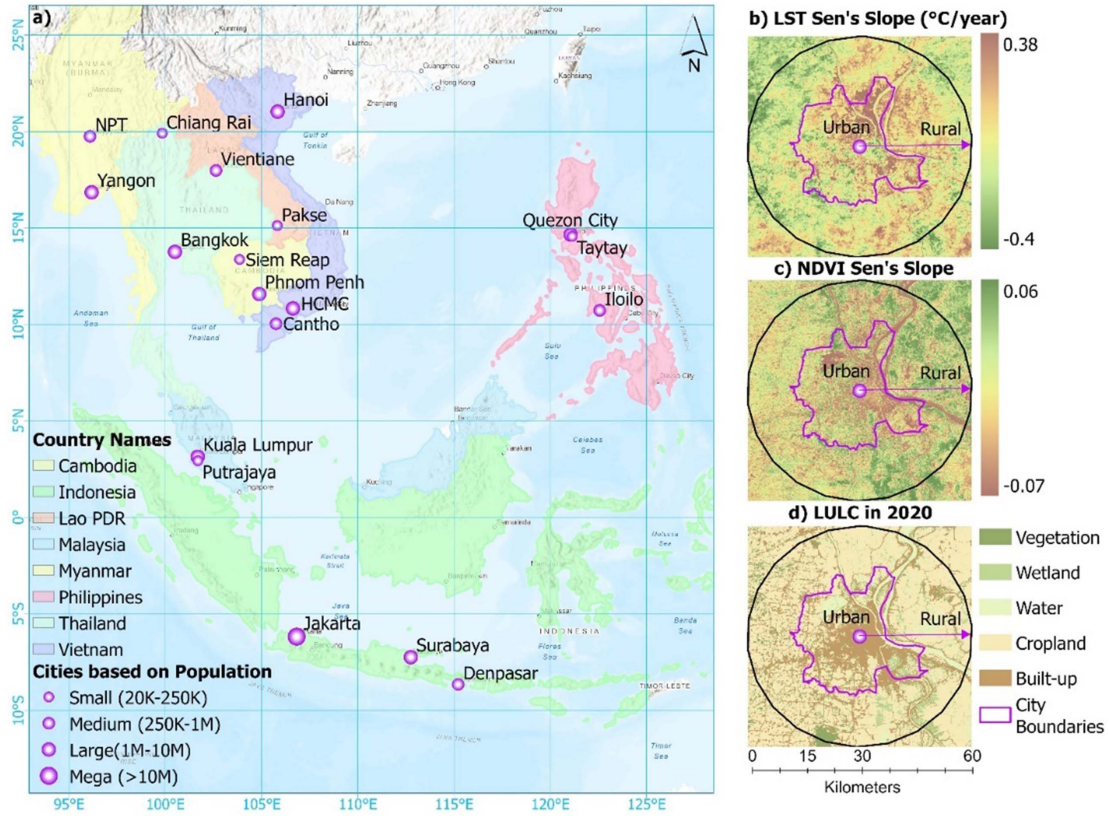


Figure 1. (a) Map of the study area showing 19 cities across 8 countries; (b) LST Sen's slope; (c) NDVI Sen's slope and (d) land use/land cover in 2020 for an example city.

Table 2. The description of the data set used in this study.

Dataset	Resolution	Sources/Methods	Year
LST changes	30 m	Landsat-based Statistical Mono-Window algorithm	2000–2022
NDVI	30 m	Landsat 5/7/8/9	2000–2022
LCLU	30 m	University of Maryland	2000, 2005, 2010, 2015, 2020

mountains exceeding 100 m above mean elevation to minimize topography effects on LST to ensure that the thermal changes reflect urban development rather than elevation-related climatic variations [14, 32]. These exclusions were implemented to ensure fair comparisons and reduce the influence of elevation on the analysis.

The data analysis was conducted across three hierarchy levels: (1) the entire study area, encompassing all 19 cities; (2) city size categories (mega, large, medium, and small); and (3) each individual city. We used the Mann–Kendall trend analysis to calculate Sen's slope for each pixel, capturing the change rate in LST and NDVI between 2000 and 2022 [33]. We then

assigned the mean values of LST and NDVI's Sen's slope to each ring buffer according to these analysis units. Subsequently, we calculated fractions of LCLU types (built-up lands, cropland, wetland, and vegetation) within each ring buffer for 2000, 2005, 2010, 2015, and 2020. Sen's slope for LCLU fractions was calculated to assess the impact of LCLU changes on LST variations. For the entire study area, we aggregated the mean values of LST, NDVI, and LCLU fraction Sen's slope across all 19 cities for a specific ring buffer. At the city size level, such as for large cities, we aggregated the values from all ring buffers corresponding to large cities.

We defined the turning points of LST Sen's slope across different city sizes. These are the locations along the URC gradient where the trend significantly shifts direction, such as changing from an increasing to a decreasing pattern or vice versa. Univariate regression models quantified the relationships between LST Sen's slope, NDVI, and LCLU changes across URCs and city size categories.

3. Results

3.1. LCLU along the URCs

We analyzed LCLU fractions within each buffer zone over two decades (figure 2). Built-up and cropland areas were the dominant LCLU types across the 19 cities, with vegetation covering over 15% of the total area (figure 2(a)). From 2000 to 2020, built-up areas increased from 28.70% to 41.19%, while cropland decreased from 36.39% to 31.38%. Urbanization primarily drove these shifts, expanding built-up land while reducing cropland and vegetation. LCLU changes followed a logarithmic pattern along the urban-rural gradient (figure 2(b)). Built-up land decreased logarithmically from urban to rural areas, while cropland, wetlands, and vegetation increased. These changes were more pronounced near urban centers and leveled off, approaching rural areas.

City size influenced LCLU patterns. In the megacity, built-up land decreased exponentially from urban to rural areas, with distinct LCLU trends compared to large, medium, and small cities, which followed patterns like the overall study area. We compared urbanization degrees and development rates using 2022 LCLU fractions and their Sen's slope. Built-up areas were the predominant LCLU type, with mean fractions of 82.14%, 54.33%, 26.27%, and 29.51% for mega, large, medium, and small cities, respectively (figure 2(b)). Urban development rates, reflected by the built-up Sen's slope, were 4.535, 3.540, 2.711, and 0.0275%/5 years for mega, large, medium, and small cities. Notably, within a 12 km radius, medium cities had the highest rate (4.778%/5 years), surpassing large cities (3.812%/5 years), megacity (1.875%/5 years), and small cities (0.0275%/5 years).

3.2. Interdependent changes with NDVI and LCLU

As shown in figure 3, we analyzed the LST Sen's slope across the urban-rural gradient within a 30 km radius for 19 cities. Urban centers did not consistently exhibit the highest LST Sen's slope, indicating disparities in LST changes from urban to rural areas, contrasting with the general LST decrease in 2022 along the gradient (figure S2). Jakarta, the only megacity, displayed a unique pattern: the LST Sen's slope gradually increased from the urban center, peaked between 16 km and 24 km, and then declined, with the city center showing no significant LST change. Large cities generally exhibited an increase followed by a decrease in the LST Sen's slope, with turning points between 6 km and 19 km, except for Hanoi, which consistently showed a decrease. Medium cities followed a decreasing–increasing–decreasing trend, with transition points between 2 km and 14 km, while small cities typically displayed a decreasing-then-increasing pattern. However, Putrajaya and Chiang Rai resembled large cities, with turning points between 3 km and 14 km.

We summarized the LST Sen's slope across 19 cities along the urban-rural gradient (figure 4). For the entire study area (figure 4(a)), the LST Sen's slope peaked at the city center (0.0303 °C/year), decreased to 3 km, and followed a bimodal pattern with peaks at 6 km and 17 km before declining. NDVI Sen's slope increased consistently from urban to rural areas, while the built-up Sen's slope mirrored the LST trend, and cropland exhibited an opposite pattern. Significant correlations were observed between the LST Sen's slope and built-up (positive, $R^2 = 0.136$), cropland, wetland, and NDVI (negative, $R^2 = 0.192$, 0.150, and 0.355, respectively). Removing the city center outlier improved correlations, particularly for built-up ($R^2 = 0.453$) and cropland ($R^2 = 0.549$).

In the megacity (figure 4(b)), the LST Sen's slope exhibited a trimodal pattern with peaks at 16 km, 20 km, and 24 km, reaching 0.127, 0.125, and 0.121 °C/year, respectively. The turning point was identified at 24 km, after which the slope declined. While the city center showed an LST Sen's slope close to 0, the rest of the megacity experienced an overall upward LST trend, indicating rapid urban warming over the past two decades. Interestingly, the NDVI Sen's slope displayed a rapidly decreasing trend from the city center, with valleys at 16 km, 20 km, and 25 km, contrasting the LST Sen's slope pattern. Built-up areas, the dominant LCLU type, initially showed an opposite trend to LST within the first 5 km but mirrored the LST pattern beyond this distance. Cropland exhibited an inverse trend to LST throughout. Regression analysis revealed significant negative correlations between the LST Sen's slope and cropland ($R^2 = 0.359$), vegetation ($R^2 = 0.153$), and NDVI ($R^2 = 0.792$). However, the positive relationship between the LST Sen's slope and wetland Sen's

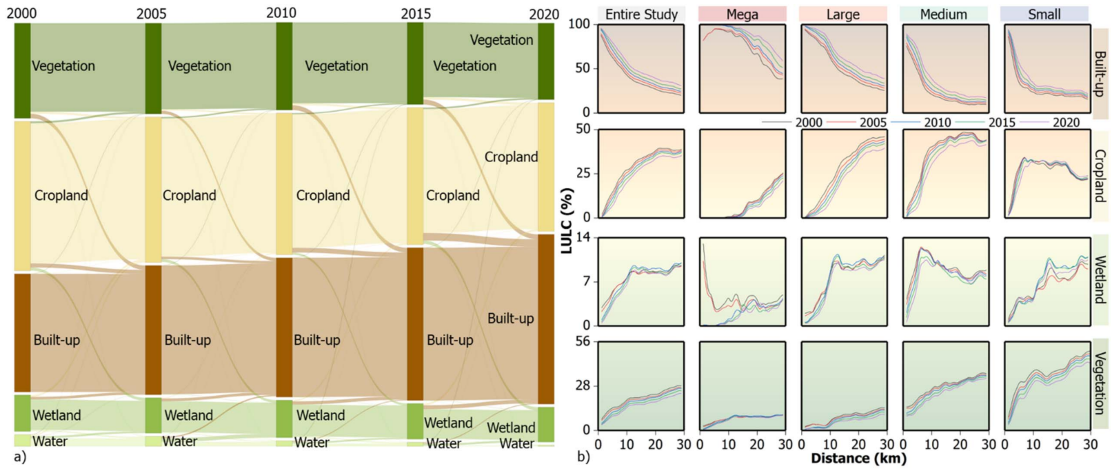


Figure 2. Land use and land cover (LCLU) changes: (a) The transition of LCLU for the entire study area, and (b) LCLU changes with different city sizes between 2000 and 2020.

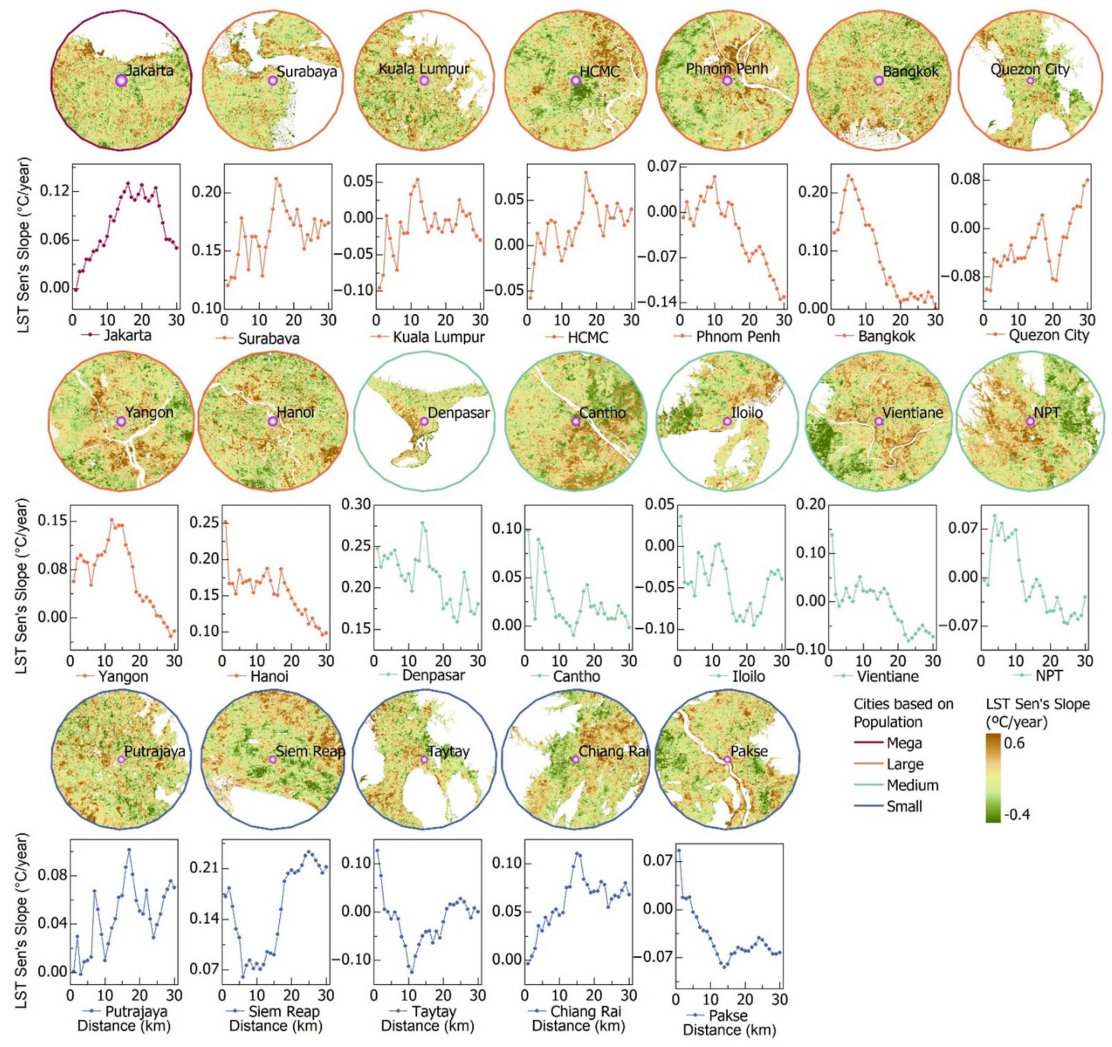


Figure 3. The spatial patterns of LST Sen's slope and their disparities from urban to rural areas by their mean values of each ring buffer for each 1 km ring buffer within a 30 km radius.

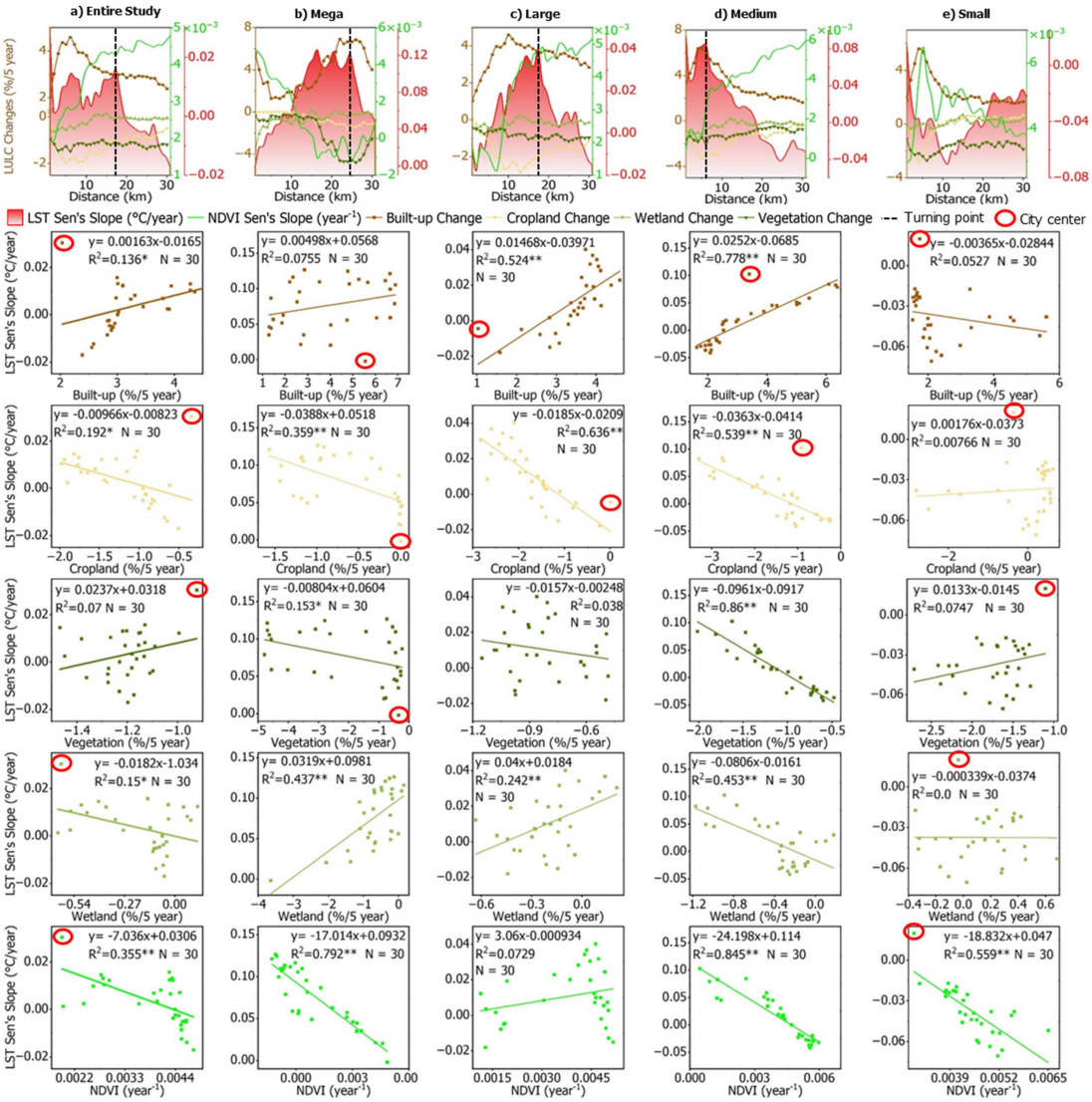


Figure 4. The patterns of LST, NDVI, and LCLU Sen's slope from urban to rural areas and their relationship at different city sizes: (a) Mega, (b) Large, (c) Medium, and (d) Small). ** and *Correlation are significant at the 0.01 and 0.05 level, respectively.

slope (less than 5% of the area) was unexpected and counterintuitive.

Large cities (figure 4(c)) exhibited a bimodal LST Sen's slope pattern, peaking at 14 km and 17 km with values of 0.0367 and 0.0401 °C/year, respectively. The turning point occurred at 17 km, after which the slope began to decline. LST showed a decline within 4 km of the center (Sen's slope < 0), while it increased between 5 km and 26 km. Unlike megacity, Built-up areas mirrored the LST trend, with a significant positive correlation ($R^2 = 0.524$), while cropland showed a significant negative correlation ($R^2 = 0.636$). Similar to those found in megacities, the positive relationship between LST and wetland Sen's slope remained counterintuitive.

Medium cities (figure 4(d)) displayed a distinct pattern, with the highest LST Sen's slope (0.103 °C/year) at the center and another peak at 6 km. LST increased up to 17 km before declining. Significant correlations were observed between LST and built-up ($R^2 = 0.778$, positive), cropland, vegetation, and NDVI ($R^2 = 0.539$, 0.860, and 0.845, negative). These LCLU and NDVI changes over time had a considerable impact on LST variations in medium cities. City center outliers were identified in the regression analysis for built-up and cropland.

Small cities (figure 4(e)) showed high LST Sen's slope values at the center (0.0199 °C/year), decreasing up to 11 km and then increasing. Apart from the city center, LST (Sen's slope < 0) has generally decreased over the past two decades. Only NDVI exhibited a significant negative correlation with LST ($R^2 = 0.559$), while no significant correlations were found for other LCLU factors. Similar to those found in medium cities, the LST Sen's slope in the city center stood out as an outlier in the regression analysis for both LCLU and NDVI.

LST in 2022 showed a consistent downward trend along the urban-rural gradient for all city sizes, reflecting typical urban heat island profiles.

Cities ranked by LST in 2022 followed the pattern: mega > large > small > medium. The mean LST Sen's slope was highest in the megacity (0.0863 °C/year), followed by large cities (0.0104 °C/year), while medium (−0.00389 °C/year) and small cities (−0.0365 °C/year) showed overall declines. Both medium and small cities experienced an overall decrease in LST, with small cities showing a faster decline than medium cities. Notably, within 12 km of the center, medium cities exhibited higher LST Sen's slope values (0.0513 °C/year) than large cities (0.01135 °C/year), reflecting dynamic urban thermal changes

In general, some cities exhibit downward LST trends (negative slope) or no LST growth (near zero slope) in certain areas, particularly around urban cores (e.g. Chiang Rai, HCMC, Iloilo, Jakarta, NPT, Phnom Penh, Putrajaya, Quezon). As shown in figure 3, green pixels in many cities indicate negative LST trends, suggesting that some areas became cooler over time. This was unexpected, as built-up areas are typically associated with rising LST due to increased population pressure, human activities, impervious surfaces, and vehicle numbers. Further investigation using fine-resolution Google Earth images from 2000 to 2020 revealed significant vegetation expansion in these areas, particularly in tree crown closures. Two key factors likely contributed to this phenomenon: (1) built-up areas were developed on non-vegetated or open land, and (2) a significant number of trees were planted early in the study period, with vegetation cover expanding over time as trees matured and their crown closures increased

4. Discussion

4.1. Changing rate of LST along the URCs and its implications

Our analysis revealed that LST change rates differ from LST patterns observed at specific times, with cities of varying sizes displaying unique LST Sen's slope patterns along the URC gradient. For the entire study area, the LST Sen's slope decreased from the city center to the 3 km buffer, where the city center exhibited the highest slope. This finding indicates that central urban areas, with higher built-up densities and lower vegetation cover, experience the most rapid LST increases over time, reflecting the intense impact of urbanization on warming.

The megacity with the highest urbanization degree and rate showed the most severe urban warming, demonstrating a severe urban warming problem over time. The LST change rate pattern showed an increasing trend in the LST Sen's slope, with trimodal peaks before declining at a turning point of around 24 km. While areas of the city center had the highest LST, they exhibited the lowest Sen's slope (close to 0). This is likely because the built-up lands, the main drivers of LST change, are already highly dense, leaving limited space for further development [11, 34]. A similar pattern was observed in large cities, with a turning point occurring at 17 km (such as Quezon city, as shown in figure S3). This suggests that urban warming around the city centers in mega and large cities has stabilized, with slight increases over time [35]. Instead, urban development is expanding outward, primarily on the outskirts of the city's core [36], leading to an increase in the LST Sen's slope up to the turning points. This pattern indicates that the urban warming effect is spreading outward and showing more widespread between city centers and turning points in mega and large cities.

Medium cities displayed distinct patterns, with the LST Sen's slope peaking at the city center, another peak at 6 km, and a consistent decline beyond. This pattern aligns with the typical urbanization process, where the city center, characterized by a high urban development rate, experiences the most rapid LST increase, subsequently influencing surrounding areas and causing a relative rise in LST over time [11, 36, 37]. Our observations indicate that LST levels in medium cities across the URCs were the lowest in 2022 (figure S2(g)). However, the LST and built-up Sen's slope increased more rapidly within a 12 km radius than large cities. Consequently, the LST Sen's slope in medium cities was significantly higher than in large cities within this range. This suggests that the LST in the core areas of medium cities has been rising substantially over time, indicating that a pronounced warming effect is rapidly developing.

Small cities exhibited patterns like medium cities, with the LST Sen's slope peaking at the city center, followed by a decline. Although small cities showed evidence of the UHI effect (figure S2), overall LST values declined over the past two decades except for a slight increase at the center. This trend can be attributed to small cities having the lowest urbanization degree and development rate. This suggests that their lower levels of urbanization and slower development rates may not contribute to the intensification of the UHI effect over time, unlike larger cities where higher urbanization has been shown to amplify the UHI effect [20, 38]. These findings align with previous research indicating that less urbanized areas tend to experience slower increases in LST and less pronounced UHI effects [37, 39].

4.2. The roles of LCLU and NDVI on LST dynamics along the URCs

While previous studies focused on LCLU impacts on urban warming at specific times [9, 15, 16], our study examined dynamic interactions between LST, LCLU, and NDVI over two decades. NDVI Sen's slope showed a robust negative correlation with LST Sen's

slope across all city sizes except large cities. NDVI captures vegetation changes, reflecting LCLU change interactions, such as vegetation or cropland conversion to built-up land during urbanization, which drives LST increases. Previous research suggested that changes in vegetation cover significantly influence urban heat dynamics [8, 11, 40]. These findings reinforce that the NDVI Sen's slope serves as a crucial indicator of the LST change rate along the URCs, supporting the role of vegetation management in mitigating urban heat effects.

Built-up areas are the predominant land cover class in SEA, and their spread clearly indicates the urbanization rate. Our study demonstrated a strong positive relationship between urban development intensity and the magnitude of the LST change rate (Sen's slope) except for the megacity (figure 4). We find that as urbanization intensifies (built-up increases over time), the LST change rate correspondingly increases, which aligns with the same ranking observed in the mean values of the LST change rate. This finding indicates that urbanization has been the driver of urban warming in SEA over the past two decades. These results are consistent with previous studies, showing that urbanization substantially intensifies local and regional land surface warming [6, 12, 41, 42].

Other LCLU types, such as vegetation and cropland, showed significant negative correlations with the LST Sen's slope. As shown in table S2, the correlation matrix highlights a strong negative correlation between built-up and ecological parameters (i.e. vegetation, wetland, and cropland), indicating that urbanization's impact on LST is driven not only by increased built-up areas but also by the concurrent reduction in these land cover types. This interconnected effect reinforces the typical UHI pattern [31, 37, 43, 44]. These findings highlight that the combined human activities and green biomass are key drivers of LST changes over time, underscoring the need for sustainable urban planning strategies that balance development with green space preservation and restoration.

We observed that the megacity, which had the highest urbanization rate (Sen's slope) and degree (built-up fraction), behaved as an exception, displaying an opposite trend in the LST Sen's slope within the first 5 km. This suggests that even though the city center of the megacity may experience less built-up increase, it still sees higher LST increases over time, attributed to the interplay between reduced vegetation cover and increased built-up density, which alter the urban energy balance through decreased evapotranspiration and enhanced heat storage effects [34, 45]. Even a small scale additional built-up development in such areas can substantially intensify urban warming [46]. Therefore, urban development should balance urbanization and warming by adopting strategies such as redirecting growth from larger cities to smaller surrounding cities or shifting development from urban centers to rural areas.

Our analysis shows that the wetland Sen's slope (consistently below zero) increased from the city center to 16 km in the megacity and 12 km in large cities, aligning with LST Sen's slope trends. This pattern resulted in a positive relationship between LST and wetland in these cities. Wetland expansion is normally associated with conversion from regular land categories to vegetation associated with water bodies, inundated areas, aquaculture farms, or flooded tall grasses. In general, water bodies are much slower to cool down than land areas are. This explains why wetland gain has led to a slight increase in temperatures, especially during early morning hours. Meanwhile, given the limited wetland coverage (less than 5% of the landscape), this wetland growth is unlikely to create a significant warming effect on LST. Thus, despite the observed positive correlation, this relationship likely reflects spatial patterns rather than a direct ecological influence.

Urbanization is a major driver of LST and NDVI trends; however, global climate change may have also contributed. Studies indicate that SEA's LST has recently risen by 0.1 °C to 0.3 °C per decade [47]. Climate change has similarly influenced NDVI, with extended growing seasons and rising temperatures linked to increased greenness. Between 2001 and 2018, greenness trends in mainland SEA and Yunnan Province, China, showed positive slopes of 0.0019 [48]. As shown in figure 4, even after accounting for climate change effects, urbanization continues to significantly drive LST increases and NDVI reductions, reinforcing its substantial impact on regional environmental changes.

5. Conclusion

This study investigated the effects of urbanization on urban thermal variations across URCs in SEA over the past two decades. Our findings revealed distinct LST change patterns across varying city sizes, with larger cities experiencing broader and more intense urban warming that extends into rural areas. While urbanization significantly contributed to urban warming in SEA, our results show that NDVI had a stronger influence on LST trends. The impact from green vegetation biomass reflects its cooling effect via evapotranspiration and shading, and the warming effect from vegetation loss due to urban expansion. Notably, some urban areas experienced a decline in heat due to increased tree crown closure over time. We recommend urban development strategies that balance urbanization and warming, such as promoting growth in smaller surrounding cities and encouraging outward expansion from densely populated urban centers into rural areas.

Data availability statement

All data used in this study are publicly available. LCLU datasets are from the Global Land Cover and Land Use Change dataset available at https://glad.umd.edu/dataset/GLCLUC2020. Landsat images are accessed through the GEE platform (https://earthengine.google.com/). Derived datasets, including the LST for 2022, LST Sen's slope, and NDVI Sen's slope from 2000 to 2022 for the 19 cities, are available on Zenodo at https://doi.org/10.5281/zenodo.14171803.

Acknowledgment

This work is funded by NASA (NASA Grant #: 80NSSC24K0920). Partial financial assistance is also provided by the Meadows Center for Water and the Environment.

ORCID iDs

Yuanhui Zhu https://orcid.org/0000-0002-0474-5945
Soe W Myint https://orcid.org/0000-0001-7809-1211
Jiquan Chen https://orcid.org/0000-0003-0761-9458
Peilei Fan https://orcid.org/0000-0003-4448-4281
Karen C Seto https://orcid.org/0000-0002-4928-2446
Atul Jain https://orcid.org/0000-0002-4051-3228
Jiaguo Qi https://orcid.org/0000-0002-8183-0297
Jin Wang https://orcid.org/0000-0003-2584-9644

References

[1] Oanh N T K and Huy L N 2024 Atmospheric emissions from electricity generation in Southeast Asia: development trend and policy responses *Curr. Pollut. Rep.* **10** 54–69
[2] Dahiya B 2014 Southeast Asia and sustainable urbanization *Glob. Asia* **9** 84–91
[3] Patwary M M *et al* 2024 Impact of extreme weather events on mental health in South and Southeast Asia: a two decades of systematic review of observational studies *Environ. Res.* **250** 118436
[4] Cianconi P, Betrò S and Janiri L 2020 The impact of climate change on mental health: a systematic descriptive review *Frontiers Psychiatry* **11** 490206
[5] Amnuaylojaroen T, Parasin N and Limsakul A 2024 Projections and patterns of heat-related mortality impacts from climate change in Southeast Asia *Environ. Res. Commun.* **6** 035019
[6] Zhou D, Xiao J, Frolking S, Zhang L and Zhou G 2022 Urbanization contributes little to global warming but substantially intensifies local and regional land surface warming *Earth's Future* **10** e2021EF002401
[7] Shen P, Zhao S, Ma Y and Liu S 2023 Urbanization-induced Earth's surface energy alteration and warming: a global spatiotemporal analysis *Remote Sens. Environ.* **284** 113361
[8] Chakraborty T and Lee X 2019 A simplified urban-extent algorithm to characterize surface urban heat islands on a global scale and examine vegetation control on their spatiotemporal variability *Int. J. Appl. Earth Obs. Geoinf.* **74** 269–80
[9] Naikoo M W, Islam A R M T, Mallick J and Rahman A 2022 Land use/land cover change and its impact on surface urban heat island and urban thermal comfort in a metropolitan city *Urban Clim.* **41** 101052
[10] Sharif M M 2022 Capturing the urban opportunity in Southeast Asia (available at: https://theaseanmagazine.asean.org/article/capturing-the-urban-opportunity-in-southeast-asia/#:~:text=Moreover%2C%20urbanisation%20in%20Southeast%20Asia,and%20the%20lives%20of%20millions.&#x003E)
[11] Estoque R C, Murayama Y and Myint S W 2017 Effects of landscape composition and pattern on land surface temperature: an urban heat island study in the megacities of Southeast Asia *Sci. Total Environ.* **577** 349–59
[12] Zhu Y, Myint S W, Feng X and Li Y 2023 An innovative scheme to confront the trade-off between water conservation and heat alleviation with environmental justice for urban sustainability: the case of phoenix, Arizona *AGU Adv.* **4** e2022AV000816
[13] Parsons T 2021 The weight of cities: urbanization effects on Earth's subsurface *AGU Adv.* **2** e2020AV000277
[14] Wang C, Myint S W, Wang Z and Song J 2016 Spatio-temporal modeling of the urban heat island in the Phoenix metropolitan area: land use change implications *Remote Sens.* **8** 185
[15] Zhang H, Qi Z-F, Ye X-Y, Cai Y-B, Ma W-C and Chen M-N 2013 Analysis of land use/land cover change, population shift, and their effects on spatiotemporal patterns of urban heat islands in metropolitan Shanghai, China *Appl. Geogr.* **44** 121–33
[16] Mohan M and Kandya A 2015 Impact of urbanization and land-use/land-cover change on diurnal temperature range: a case study of tropical urban airshed of India using remote sensing data *Sci. Total Environ.* **506** 453–65
[17] Fan P *et al* 2022 Urbanization, economic development, and environmental changes in transitional economies in the global south: a case of Yangon *Ecol. Process.* **11** 65
[18] Nguyen C T, Chidthaisong A, Limsakul A, Varnakovida P, Ekkawatpanit C, Diem P K and Diep N T H 2022 How do disparate urbanization and climate change imprint on urban thermal variations? A comparison between two dynamic cities in Southeast Asia *Sustain. Cities Soc.* **82** 103882
[19] Zhou B, Rybski D and Kropp J P 2017 The role of city size and urban form in the surface urban heat island *Sci. Rep.* **7** 4791
[20] Manoli G, Fatichi S, Schläpfer M, Yu K, Crowther T W, Meili N, Burlando P, Katul G G and Bou-Zeid E 2019 Magnitude of urban heat islands largely explained by climate and population *Nature* **573** 55–60
[21] IPCC 2022 Climate Change 2022: impacts, Adaptation and Vulnerability
[22] Pahl R E 1966 The rural-urban continuum *Sociol. Rural.* **6** 299–329
[23] UN DESA 2019 *World Urbanization Prospects, The 2018 Revision* (United Nations Department of Economic and Social Affairs)
[24] Duguay-Tetzlaff A, Bento V, Göttsche F, Stöckli R, Martins J, Trigo I, Olesen F, Bojanowski J, Da Camara C and Kunz H 2015 Meteosat land surface temperature climate data record: achievable accuracy and potential uncertainties *Remote Sens.* **7** 13139–56
[25] Freitas S C, Trigo I F, Macedo J, Barroso C, Silva R and Perdigão R 2013 Land surface temperature from multiple geostationary satellites *Int. J. Remote Sens.* **34** 3051–68
[26] Sun D, Pinker R T and Basara J B 2004 Land surface temperature estimation from the next generation of geostationary operational environmental satellites: GOES M–Q *J. Appl. Meteorol. Climatol.* **43** 363–72
[27] Li Z-L, Tang B-H, Wu H, Ren H, Yan G, Wan Z, Trigo I F and Sobrino J A 2013 Satellite-derived land surface temperature:

current status and perspectives *Remote Sens. Environ* **131** 14–37
[28] Jesdale B M, Morello-Frosch R and Cushing L 2013 The racial/ethnic distribution of heat risk–related land cover in relation to residential segregation *Environ. Health Perspect.* **121** 811–7
[29] Morello-Frosch R and Lopez R 2006 The riskscape and the color line: examining the role of segregation in environmental health disparities *Environ. Res.* **102** 181–96
[30] Potapov P *et al* 2022 The global 2000–2020 land cover and land use change dataset derived from the landsat archive: first results *Front. Remote Sens.* **3** 856903
[31] European Space Agency 2017 Land cover CCI product user guide version 2 *Tech. Rep. In*
[32] Wang Z, Fan C, Zhao Q and Myint S W 2020 A geographically weighted regression approach to understanding urbanization impacts on urban warming and cooling: a case study of Las Vegas *Remote Sens.* **12** 222
[33] Yue S and Wang C Y 2002 Applicability of prewhitening to eliminate the influence of serial correlation on the Mann-Kendall test *Water Resour. Res.* **38** 4–1
[34] Zhou X and Chen H 2018 Impact of urbanization-related land use land cover changes and urban morphology changes on the urban heat island phenomenon *Sci. Total Environ.* **635** 1467–76
[35] Ali S, Tariq A, Kayumba P M, Zeng F, Ahmed Z, Azmat M, Mind'je R and Zhang T 2024 Local surface warming assessment in response to vegetation shifts over arid lands of Central Asia (2001–2020) *Sci. Total Environ.* **929** 172628
[36] Schneider A *et al* 2015 A new urban landscape in East–Southeast Asia, 2000–2010 *Environ. Res. Lett.* **10** 034002
[37] Zhu Y, Myint S W, Schaffer-Smith D, Muenich R L, Tong D and Li Y 2022 Formulating operational mitigation options and examining intra-urban social inequality using evidence-based urban warming effects *Front. Environ. Sci.* **9** 795474
[38] Hu X, Zhou W, Qian Y and Yu W 2017 Urban expansion and local land-cover change both significantly contribute to urban warming, but their relative importance changes over time *Landsc. Ecol.* **32** 763–80
[39] Oke T R 1982 The energetic basis of the urban heat island *Q. J. R. Meteorol. Soc.* **108** 1–24
[40] Gui X, Wang L, Yao R, Yu D and Li C A 2019 Investigating the urbanization process and its impact on vegetation change and urban heat island in Wuhan, China *Environ. Sci. Pollut. Res.* **26** 30808–25
[41] Piano E *et al* 2017 Urbanization drives community shifts towards thermophilic and dispersive species at local and landscape scales *Glob. Change Biol.* **23** 2554–64
[42] Li G, Zhang X, Mirzaei P A, Zhang J and Zhao Z 2018 Urban heat island effect of a typical valley city in China: responds to the global warming and rapid urbanization *Sustain. Cities Soc.* **38** 736–45
[43] Voogt J A and Oke T R 2003 Thermal remote sensing of urban climates *Remote Sens. Environ.* **86** 370–84
[44] Liao W *et al* 2018 Stronger contributions of urbanization to heat wave trends in wet climates *Geophys. Res. Lett.* **45** 11,310–311,317
[45] Yue W, Liu X, Zhou Y and Liu Y 2019 Impacts of urban configuration on urban heat island: an empirical study in China mega-cities *Sci. Total Environ.* **671** 1036–46
[46] Mentaschi L, Duveiller G, Zulian G, Corbane C, Pesaresi M, Maes J, Stocchino A and Feyen L 2022 Global long-term mapping of surface temperature shows intensified intra-city urban heat island extremes *Glob. Environ. Change* **72** 102441
[47] IPCC 2018 Special report on the impacts of global warming of 1.5° C above pre-industrial levels and related global greenhouse gas emission pathways, in the context of strengthening the global response to the threat of climate change *Sustainable Development, and Efforts to Eradicate Poverty* vol **32**
[48] Fan F, Xiao C, Feng Z and Yang Y 2023 Impact of human and climate factors on vegetation changes in mainland southeast asia and yunnan province of China *J. Clean. Prod.* **415** 137690